Energy loss of ions and ion clusters in a disordered electron gas

Hrachya B. Nersisyan[1,*] and Amal K. Das[2,†]
[1]*Theoretical Physics Division, Institute of Radiophysics and Electronics, Ashtarak-2, 378410, Armenia*
[2]*Department of Physics, Dalhousie University, Halifax, Nova Scotia B3H 3J5, Canada*
(Received 26 September 2003; published 27 April 2004)

The various aspects of the correlated stopping power of pointlike and extended ions moving in a disordered degenerate electron gas have been analytically and numerically studied. Within the linear response theory we have made a systematic and comprehensive investigation of correlated stopping power, vicinage function, and related quantities for protons and extended ions, as well as for their clusters. The disorder, which leads to a damping of plasmons and quasiparticles in the electron gas, is taken into account through a relaxation time approximation in the linear response function. The stopping power for an arbitrary extended ion with a single bound electron is calculated in both the low- and high velocity limitsy. Our analytical results show that in a high velocity limit the main logarithmic contribution to the stopping power for an extened ion is significantly modified and for instance, in the case of He^+, Li^{2+}, and Be^{3+} ions must behave as $\ln(Av^5)$, $\ln(Av^{3.25})$, and $\ln(Av^{2.77})$, respectively where v is the ion velocity. This behavior may be contrasted with the usual $\ln(v^2)$ dependence for a point ion projectile. It is shown that the factor A which depends on the damping can be significantly reduced by increasing the latter. In order to highlight the effects of damping we present a comparison of our analytical and numerical results, in the case of both pointlike and extended ions, obtained for a nonzero damping with those for a vanishing damping.

DOI: 10.1103/PhysRevE.69.046404 PACS number(s): 52.40.Mj, 34.50.Bw, 61.85.+p, 71.45.Gm

I. INTRODUCTION

The energy loss of a charged particle moving in a degenerate electron gas (DEG) is of continuing interest. This is a topic of direct relevance to a quantitative understanding, for instance, of beam-target interaction in the contexts of particle driven fusion [1–3] and the implantation experiments which include a modification of metal surfaces using ion beams. The valence electron system in a solid can be regarded, to a good approximation, as a DEG with a uniform electron density n_0. The energy losses of ions moving in such an electron gas can be studied through the stopping power (SP) of the medium. Following the pioneering works of Lindhard, and Lindhard and Winther [4], a lot of calculations were done within the framework of the linear response theory (see, e.g., Refs. [5–8] for reviews). The main part of these calculations was based on the linear response function in random-phase approximation (RPA) which is usually valid in the weak coupling limit of an electron gas, i.e., for the density parameter $r_s=(3/4\pi n_0 a_0^3)^{1/3}<1$, where $a_0=0.529$ $\AA$ is the Bohr radius. Electron energy band effects, electron-electron correlation beyond RPA, and electron-impurity (disorder) collisions all contribute to the linear response function and hence to the linear response theory of SP, for real solids. To include all these aspects at the same level is a formidable task. In this paper we shall consider a disordered electron gas in RPA and make a detailed study of effects of disorder on various aspects of SP.

In our work the effect of disorder is included in the linear response function within RPA through a simple, physically motivated, and number-conserving relaxation-time approximation (RTA), first considered by Mermin [9] and then by Das [10]. In this approximation the effect of disorder which leads to a damping of excitations enters the RPA dielectric function, for a given electron-impurity collision frequency γ, through $\varepsilon_{\mathrm{RPA}}(k,\omega+i\gamma)$ where γ is used as a model parameter. In some investigations of ion stopping in carbon and silicon targets, γ was determined by fitting $-\mathrm{Im}[\varepsilon^{-1}(0,\omega,\gamma)]$ to experimental optical energy loss functions [11–13]. This disorder-inclusive dielectric function, with the collision frequency as a free parameter, allows some physical insight and useful numerical estimates of the influence of disorder on energy loss in a DEG. The predicted effect is a shorter lifetime and smaller mean free path of the plasmons resulting in considerable modifications of the wake field behind the passing ion [14]. This is of particular importance for vicinity effects on the energy loss of two- [13] and multi-ion arrangements [15,16]. For the stopping of a single ion, the broadening of the plasmon peak with increasing γ shifts the threshold for the energy loss by plasmon excitation towards lower projectile velocities. It now becomes possible for low-velocity projectile ions to excite plasmons (in addition to single-particle excitations). This increases the SP at low projectile velocities, compared to the disorder-free RPA result [12]. Recently a similar study has been performed for a classical (nondegenerate) target [17], where the parameter γ is treated within the Faber-Ziman semiclassical expression including the plasma temperature effects. For a DEG and for a given electron density, the damping parameter can be assumed to be a constant to a good approximation. The damping parameter in RTA will be further commented on in Sec. V.

In an earlier work [18] we made a detailed study of the respective contributions of collective (plasmon) and single-

*Electronic address: hrachya@irphe.am
†Electronic address: akdas@da1.ca

particle excitations to SP in a disorder-free DEG and found a generalized sum rule for pointlike and extended charged projectiles and clusters. In a separate work [19] we investigated the above-mentioned respective contributions to SP for pointlike and extended projectiles in a disordered DEG within the linear response formulation, the effects of disorder being taken included through a number-conserving RTA. The present work, which is a natural sequel to but goes beyond [18,19], reports on our investigations of the individual (ISP) and correlated (CSP) stopping powers of pointlike and extended ions as well as their clusters in a disordered DEG. Previously the CSP has been considered for diclusters and within a simple plasmon-pole approximation [20] and more recently in the context of an inertial confinement fusion scenario using the full Lindhard (i.e., RPA) dielectric function and a variety of analytical and numerical methods (see, e.g., Refs. [1,3,6,7,15,16,21,22] for reviews). In the studies presented in this paper we use the full RPA dielectric function and include damping through a number-conserving RTA for a DEG medium [9,10]. The plan of the paper is follows. In Sec. II we briefly outline the linear response formulation for SP of a dicluster of identical extended ions and use analytical expressions for the disorder-inclusive dielectric function derived in Ref. [19]. The dicluster SP formulation is then extended to an N cluster system through a binary superposition. As in Refs. [18,19,23] we consider proton (as a pointlike projectile) and an extended ion of arbitrary nuclear charge Z but having a single bound electron, as well as proton and N $(N \geqslant 2)$ extended ion clusters. As useful examples of extended projectiles we consider He^+, Li^{2+}, and Be^{3+} ions, and He^+ ion N clusters. In Sec. III we develop some analytical techniques to calculate the SP of an extended ion in low- and high-velocity regimes. The two particular cases studied in this section are (i) low-velocity limit for extended ion SP moving in a damping-free ($\gamma=0$) DEG, and (ii) high-velocity limit for arbitrary disorder (or γ). Section IV contains systematic numerical calculations for the SP and the vicinage function. The results are summarized and discussed in Secs. IV and V.

II. STOPPING POWER: PRELIMINARIES

A. SP of an ion dicluster

Consider an external charge with distribution $\rho_{\rm ext}(\mathbf{r},t) = Q_{\rm ext}(\mathbf{r}-\mathbf{v}t)$ moving with velocity $\mathbf{v}$ in a medium characterized by the longitudinal dielectric function $\varepsilon(k,\omega,\gamma)$. Within the linear response theory and in the Born approximation the scalar electric potential $\varphi(\mathbf{r},t)$ due to this external charge screened by the medium is given by [4,24]

$$\varphi(\mathbf{r},t) = \frac{4\pi}{(2\pi)^3}\int d\mathbf{k} G(\mathbf{k}) \frac{\exp[i\mathbf{k}\cdot(\mathbf{r}-\mathbf{v}t)]}{k^2\varepsilon(k,\mathbf{k}\cdot\mathbf{v},\gamma)}, \qquad (1)$$

where $G(\mathbf{k})$ is the Fourier transform of the stationary charge $Q_{\rm ext}(\mathbf{r})$.

The stopping power which is the energy loss of the external charge regarded as a projectile, per unit path length in the medium regarded as a target material, can be calculated from the force acting on the charge. The latter is related to the induced electric field $\mathbf{E}_{\rm ind}$ in the medium. For a three-dimensional medium we have, for the SP (see, e.g., Refs. [6–8] and references therein),

$$S \equiv -\int d\mathbf{r} Q_{\rm ext}(\mathbf{r}-\mathbf{v}t)\frac{\mathbf{v}}{v}\mathbf{E}_{\rm ind}(\mathbf{r},t)$$
$$= \frac{1}{2\pi^2 v}\int d\mathbf{k}|G(\mathbf{k})|^2 \frac{\mathbf{k}\cdot\mathbf{v}}{k^2}{\rm Im}\frac{-1}{\varepsilon(k,\mathbf{k}\cdot\mathbf{v},\gamma)}. \qquad (2)$$

Equation (2) is applicable to any external charge distribution. We shall apply it to a dicluster of two identical ions with fixed nuclear charge Ze and one bound electron on each ion, moving in a disordered DEG at a given velocity $\mathbf{v}$. It is assumed that the pointlike nuclei are separated by a variable distance R, and ϑ is the angle between the interionic separation vector $\mathbf{R}$ and the velocity vector $\mathbf{v}$. For the projectile system under study we may write $Q_{\rm ext}(\mathbf{r})$ as

$$Q_{\rm ext}(\mathbf{r}) = Ze[\delta(\mathbf{r}) + \delta(\mathbf{r}-\mathbf{R})] - e[\rho(\mathbf{r}) + \rho(|\mathbf{r}-\mathbf{R}|)]. \qquad (3)$$

For point-ions, only the delta-function terms in Eq. (3) need be considered while for an extended-charge projectile all the terms in Eq. (3) are included. $\rho(r)$ is the spatial distribution, assumed to be spherically symmetric, of bound electrons in the ions.

We use a 1s-type wave function of the form $\psi_{1s}(r) = (Z^3/\pi a_0^3)^{1/2}\exp(-Zr/a_0)$ to describe the bound electron on each ion, with a_0 the Bohr radius. It may be remarked that, unlike in the work of Wang and Nagy [23], we are considering an unscreened 1s electron. The Fourier transform of the spatial distribution $\rho(r)=|\psi_{1s}(r)|^2$ is then expressed as $\rho(k) = (1+k^2a_0^2/4Z^2)^{-2}$.

For a dicluster of two identical ions we have

$$|G(\mathbf{k})|^2 = 2e^2[Z-\rho(k)]^2[1+\cos(\mathbf{k}\cdot\mathbf{R})]. \qquad (4)$$

From Eqs. (2) and (4) the SP of this two-ion system is then found to be [19]

$$S(\lambda,R,\vartheta) = 2S_{\rm ind}(\lambda) + 2S_{\rm corr}(\lambda,R,\vartheta), \qquad (5)$$

where $S_{\rm ind}(\lambda)$ and $S_{\rm corr}(\lambda,R,\vartheta)$ stand for individual and correlated SP, respectively,

$$S_{\rm ind}(\lambda) = \frac{16Z^2\Sigma_0}{\pi^3\chi^4\lambda^2}\int_0^\infty \mathcal{Z}^2(\alpha,z)z dz \int_0^\lambda {\rm Im}\frac{-1}{\varepsilon(z,u,\Gamma)}u du, \qquad (6)$$

$$S_{\rm corr}(\lambda,R,\vartheta) = \frac{16\,Z^2\Sigma_0}{\pi^3\chi^4\lambda^2}\int_0^\infty \mathcal{Z}^2(\alpha,z)z dz \int_0^\lambda {\rm Im}\frac{-1}{\varepsilon(z,u,\Gamma)}u du$$
$$\times \cos\left(\frac{2uz}{\lambda}\xi\cos\vartheta\right) J_0\left(2\xi z \sin v\sqrt{1-\frac{u^2}{\lambda^2}}\right). \qquad (7)$$

$J_0+(x)$ is the Bessel function of first kind and zero order, $\Sigma_0 = e^2/2a_0^2 \simeq 2.566$ GeV/cm. Here we have introduced the dimensionless Lindhard variables $z=k/2k_F$, $u=\omega/kv_F$, where v_F and k_F are, respectively, the Fermi velocity and wave number of the target electrons, $\lambda = v/v_F$, $\xi = k_F R$. $\mathcal{Z}(\alpha,z) = 1-Z^{-1}\rho(\alpha,z)$, where $\alpha = \pi\chi^2 Z$, $\chi^2 = 1/\pi k_F a_0$

$=(4/9\pi^4)^{1/3}r_s$, and $\rho(\alpha,z)$ is the Fourier transform of the spatial distribution of bound electron in the ion written in the Lindhard variables z and u. With the notations introduced above we have

$$\rho(\alpha,z)=\frac{\alpha^4}{(\alpha^2+z^2)^2}. \tag{8}$$

We briefly note that in Eq. (5) the term for correlated stopping power (CSP) $S_{\rm corr}$ vanishes for large R ($R\to\infty$) and SP is then the sum of individual stopping powers (ISP) for the separate ions. For $R\to 0$ the two ions coalesce into a single entity. Then $S_{\rm corr}=S_{\rm ind}$ and SP is that for a total charge $2eZ_t=2e(Z-1)$.

Let us now specify the disorder-inclusive dielectric function. The target medium is assumed to be disordered due to impurities, etc., with which the target electrons will undergo collisions. The effect of disorder on the RPA dielectric function $\varepsilon_{\rm RPA}(k,\omega)$ is included, in a number-conserving approximation, through a relaxation time $\tau=1/\gamma$ where γ is the collision frequency [9,10]. For $\tau\to\infty$ this linear response function $\varepsilon(k,\omega,\gamma)$ reduces to the usual Lindhard dielectric function. With the notations introduced in the preceding paragraph, $\varepsilon(k,\omega,\gamma)$ reads

$$\varepsilon(z,u,\Gamma)=1+\frac{(zu+i\Gamma)[\varepsilon_{\rm RPA}(z,u,\Gamma)-1]}{zu+i\Gamma[\varepsilon_{\rm RPA}(z,u,\Gamma)-1]/[\varepsilon_{\rm RPA}(z,0)-1]}, \tag{9}$$

where $\Gamma=\hbar\gamma/4E_F$, E_F being the Fermi energy $=\hbar^2k_F^2/2m$ with m as the effective mass. The quantity γ (or Γ) is a measure of damping of excitations in the disordered electron gas. $\varepsilon_{\rm RPA}(z,u,\Gamma)=\varepsilon_{\rm RPA}(k,\omega+i\gamma)$ is the longitudinal dielectric function of a zero-temperature (degenerate) electron gas in RPA. $\varepsilon_{\rm RPA}(z,0)=\varepsilon_{\rm RPA}(k,0)$ is the static dielectric function. The explicit analytical expression for $\varepsilon_{\rm RPA}(z,u,\Gamma)$ has been derived in Ref. [19], which we recall here for completeness:

$$\begin{aligned}\varepsilon_{\rm RPA}(z,u,\Gamma)&=\varepsilon_{\rm RPA}(k,\omega+i\gamma)\\&=1+\frac{\chi^2}{z^2}[f_1(z,u,\Gamma)+if_2(z,u,\Gamma)],\end{aligned} \tag{10}$$

where we have introduced the functions $f_1(z,u,\Gamma)$ and $f_2(z,u,\Gamma)$ as in the usual RPA expression of longitudinal dielectric function,

$$\begin{aligned}f_1(z,u,\Gamma)=\frac{1}{2}+\frac{1}{16z^3}\{&[z^2(U_-^2-1)-\Gamma^2]Y_1(z,U_-)\\&-[z^2(U_+^2-1)-\Gamma^2]Y_1(z,U_+)\\&+4\Gamma z[U_+Y_2(z,U_+)-U_-Y_2(z,U_-)]\},\end{aligned} \tag{11}$$

$$\begin{aligned}f_2(z,u,\Gamma)=\frac{1}{8z^3}\{&\Gamma z[U-Y_1(z,U_-)-U_+Y_1(z,U_+)]+[z^2(U_-^2\\&-1)-\Gamma^2]Y_2(z,U_-)-[z^2(U_+^2-1)-\Gamma^2]Y_2(z,U_+)\}\end{aligned} \tag{12}$$

with $U_\pm=u\pm z$,

$$Y_1(z,U)=\ln\frac{z^2(U+1)^2+\Gamma^2}{z^2(U-1)^2+\Gamma^2}, \tag{13}$$

$$Y_2(z,U)=\arctan\frac{z(U-1)}{\Gamma}-\arctan\frac{z(U+1)}{\Gamma}. \tag{14}$$

In the case of vanishing damping ($\gamma\to 0$ and $\Gamma\to 0$) the expressions (9)–(14) coincide with the Lindhard result [4].

In many experimental situations, clusters of ions are formed with random orientations of **R**. A correlated stopping power appropriate to this situation may be obtained by carrying out a spherical average over **R** of $S_{\rm corr}$ in Eq. (7). We find

$$\begin{aligned}\overline{S}_{\rm corr}(\lambda,R)&\\&=\frac{16Z^2\Sigma_0}{\pi^3\chi^4\lambda^2}\int_0^\infty \mathcal{Z}^2(\alpha,z)j_0(2z\xi)zdz\int_0^\lambda {\rm Im}\frac{-1}{\varepsilon(z,u,\Gamma)}udu,\end{aligned} \tag{15}$$

where $j_0(x)=\sin(x)/x$.

One may consider an interference or vicinage function which is a measure of the difference between the individual-particle contribution and its correlated counterpart to the stopping power. This function is defined as [20]

$$g(\lambda,R,\vartheta)=\frac{S_{\rm corr}(\lambda,R,\vartheta)}{S_{\rm ind}(\lambda)}, \tag{16}$$

$$g_{\rm av}(\lambda,R)=\frac{\overline{S}_{\rm corr}(\lambda,R)}{S_{\rm ind}(\lambda)}. \tag{17}$$

Equation (5) can then be put in the form

$$S(\lambda,R,\vartheta)=2S_{\rm ind}(\lambda)[1+g(\lambda,R,\vartheta)], \tag{18}$$

whence

$$S_{\rm av}(\lambda,R)=2S_{\rm ind}(\lambda)[1+g_{\rm av}(\lambda,R)]. \tag{19}$$

$g(\lambda,R,\vartheta)$ describes the extent of correlation effects with respect to an uncorrelated scenario. The vicinage function becomes equal to unity as $R\to 0$ when the two ions coalesce into an single entity, and goes to zero as $R\to\infty$ when the two ions are totally uncorrelated.

B. SP of a linear *N*-ion chain

In many situations, e.g., in the interaction of an ion beam with a target medium, several ions are stopped simultaneously. This naturally raises the question of correlation effects due to mutual influence of the ions in a given ion configuration. Some interesting candidates for these correlation

effects are, for instance, the ion clouds created by very fast fragmentation and ionization (on a femtosecond scale) of large clusterions when passing through a target. A possible stopping enhancement for such large clusters is important in connection with the proposed use of cluster-ion beams for inertial confinement fusion as mentioned in the Introduction. As in the case of single ion stopping, the whole slowing down process of some arrangement of ions involves the SP, the charge states of the ions, and—as an additional aspect—the Coulomb explosion of these clouds of ions driven by the mutual repulsion among the charges. A complete description of the stopping of these ion clusters requires a simultaneous treatment of all these including correlation effects on both the SP and the charge state. In this paper we do not discuss the charge state evolution of the projectiles under study, but concentrate on the ion-ion correlation effects with respect to the SP for a given ion configuration, i.e., for given relative positions and charges of the ions at some instant in their slowing down process.

With this proviso and going beyond an extended ion and a dicluster, we now consider the energy loss of a linear ion beam projectile modelled by a chain of N ions each of which moving with velocity $\mathbf{v}$. In this study we restrict ourselves to a simple geometry for the chain, which assumes a nearest-neighbor distance R having an orientation angle ϑ with respect to the ion velocity vector $\mathbf{v}$. This ion configuration has been intensively explored in earlier works (see, e.g., Refs. [1,15,16,21] and references therein) and can be viewed as a useful model to describe the overall (averaged) behavior of ion distributions as produced in the fragmentation process of cluster ions when impacting a target. Furthermore, it allows for relatively easy analytical and numerical calculations.

We can apply Eq. (5)–(7) to any selected pair of ions within a given configuration of N-ions Considering this configuration to be an N-ion chain the energy loss for the chain is obtained as a linear superposition of the corresponding quantity for a dicluster, and is given by

$$S_N(\lambda,R,\vartheta) = NS_{\rm ind}(\lambda) + 2\sum_{n=1}^{N-1}(N-n)S_{\rm corr}(\lambda,nR,\vartheta)$$
$$= \frac{16Z^2\Sigma_0}{\pi^3\chi^4\lambda^2}\int_0^\infty \mathcal{Z}^2(\alpha,z)zdz\int_0^\lambda {\rm Im}\frac{-1}{\varepsilon(z,u,\Gamma)} \times \Upsilon_N(z,u,\vartheta)\, udu. \qquad (20)$$

Here $\Upsilon_N(z,u,\vartheta)$ is the structure factor of the linear N-ion chain which depends on N and the orientation angle ϑ. For such a structure we expect a strong dependence of the SP on the orientation of the chain with respect to its velocity. For velocities parallel to the chain, that is for $\mathbf{R}\|\mathbf{v}$ ($\vartheta=0$), the correlations between ions are maximal [15,16,21] and the structure factor Υ_N is then given by

$$\Upsilon_N(z,u) \equiv \Upsilon_N(z,u,0) = \left[\frac{\sin(Nzu\xi/\lambda)}{\sin(zu\xi/\lambda)}\right]^2. \qquad (21)$$

In Eq. (20) $S_{\rm ind}(\lambda)$ and $S_{\rm corr}(\lambda,nR,\vartheta)$ stand for individual and two-ion correlated SP's and are given by Eqs. (6) and (7), respectively. We again briefly note that the correlated SP for the chain vanishes for large R ($R\to\infty$) and the SP is the sum of individual ion SP's, $S_N\to NS_{\rm ind}(\lambda)$.For $R\to 0$ we have $S_{\rm corr}(\lambda,R,\vartheta)\to S_{\rm ind}(\lambda)$ and the SP is then that for a resulting cluster of charge: $S_N\to N^2S_{\rm ind}(\lambda)$.

III. STOPPING POWER: THEORETICAL CALCULATIONS

The most characteristic features of a charged projectile are its charge strength and structure, and the velocity v. One sees from Eqs. (5)–(7) that the stopping power of any extended projectile with effective charge $Z_{\rm eff}=Z-\rho(\alpha,z)$ grows quadratically with $Z_{\rm eff}$. This is a consequence of the linear response approach which depends quadratically on the perturbation $Z_{\rm eff}$. However, even under these circumstances, for extended projectiles the dependence of SP on the projectile charge Z (or the dependence on the total charge $Z_t=Z-1$) is more complicated than for pointlike ions, as can be seen from Eqs. (5)–(7). In this context it may be recalled that within the linear response theory but for a classical or partially degenerate electron gas medium, the classical Bohr result with the upper cutoff parameter $k_{\rm max}=mv^2/|Z|e^2$ (which depends on the ionic charge Z) leads to a SP behaving as $Z^2\ln(1/|Z|)$ for large velocities (see, e.g., Ref. [6]). In our case with a fully quantum RPA dielectric function ($T=0$) the high-velocity energy loss is given by the Bethe expression $Z^2\ln(2mv^2/\hbar\omega_p)$ where ω_p is the plasmon frequency. This logarithmic factor does not depend on the ionic charge Z. Besides, as we show below the dependence on the velocity in the high-velocity limit is more involved than its low-velocity counterpart. In this section we will derive some analytical expressions for SP of extended ions in low- and high-velocity limits with special attention given to the ISP.

A. Low-velocity limit: General formulation

Let us consider SP for slow projectiles. A consequence of the linear response theory, confirmed by experiments, is that for ion velocities v low compared to the Fermi velocity v_F, the stopping power is proportional to v (see, e.g., the latest experiment [25]). The coefficient of proportionality may be called a friction coefficient. Using analytical results obtained for $\varepsilon_{\rm RPA}(z,u,\Gamma)$ the general expressions for SP follow from Eqs. (5)–(14):

$$S_{\rm ind}(\lambda) \simeq \frac{8Z^2\Sigma_0}{3\pi^2\chi^2}\lambda\int_0^\infty \frac{\mathcal{Z}^2(\alpha,z)\Xi(z,\Gamma)z^3dz}{[z^2+\chi^2 f(z)]^2} = \frac{8Z^2\Sigma_0}{3\pi^2\chi^2}\lambda\mathcal{R}_{\rm ind}(\alpha,\Gamma,\chi^2), \qquad (22)$$

$$S_{\rm corr}(\lambda,R,\vartheta) \simeq \frac{4Z^2\Sigma_0}{\pi^2\chi^2}\lambda\int_0^\infty \frac{\mathcal{Z}^2(\alpha,z)\Xi(z,\Gamma)z^3dz}{[z^2+\chi^2 f(z)]^2}[\Phi_1(z\xi) + \Phi_2(z\xi)\sin^2\vartheta], \qquad (23)$$

$$\overline{S_{\rm corr}}(\lambda,R) \simeq \frac{8Z^2\Sigma_0}{3\pi^2\chi^2}\lambda\int_0^\infty j_0(2z\xi)\frac{\mathcal{Z}^2(\alpha,z)\Xi(z,\Gamma)z^3dz}{[z^2+\chi^2 f(z)]^2}, \tag{24}$$

where the dimensionless friction coefficient $\mathcal{R}_{\rm ind}(\alpha,\Gamma,\chi^2)$ depends on both the target and projectile properties and hence also on the dimensionless damping parameter Γ. We have introduced the following functions:

$$\Xi(z,\Gamma) = \frac{2z}{\pi\Gamma}\frac{f(z)[f(z)-\psi(z,\Gamma)]}{\psi(z,\Gamma)}, \tag{25}$$

$$\Phi_1(\xi) = \frac{1}{\xi^3}\left[\left(\xi^2-\frac{1}{2}\right)\sin(2\xi)+\xi\cos(2\xi)\right], \tag{26}$$

$$\Phi_2(\xi) = \frac{1}{\xi^3}\left[\left(\frac{3}{4}-\xi^2\right)\sin(2\xi)-\frac{3}{2}\xi\cos(2\xi)\right], \tag{27}$$

$$\psi(z,\Gamma) = \frac{1}{2}+\frac{1}{8z^3}\left\{[z^2(z^2-1)-\Gamma^2]\ln\frac{z^2(z-1)^2+\Gamma^2}{z^2(z+1)^2+\Gamma^2} - 4\Gamma z^2\left(\arctan\frac{z^2+z}{\Gamma}-\arctan\frac{z^2-z}{\Gamma}\right)\right\}, \tag{28}$$

$$f(z) = \psi(z,0) = \frac{1}{2}+\frac{1-z^2}{4z}\ln\left|\frac{1+z}{1-z}\right|. \tag{29}$$

From Eqs. (26) and (27) it follows that $\Phi_1(\xi)\to 2/3$ and $\Phi_2(\xi)\to 0$ at $\xi\to 0$. Consequently, as expected, $S_{\rm corr}(\lambda,R,\vartheta)\to S_{\rm ind}(\lambda)$ when $R\to 0$. Since in the low-velocity limit both ISP and CSP are proportional to the velocity of the projectile the vicinage function $g(\lambda,R,\vartheta)$ at $\lambda\ll 1$ depends only on the interionic distance R and orientation angle ϑ.

When the damping vanishes ($\Gamma\to 0$) Eq. (28) becomes

$$\psi(z,\Gamma)\to f(z)-\frac{\pi\Gamma}{2z}\theta(1-z)+O(\Gamma^2), \tag{30}$$

where $\theta(z)$ is the Heaviside unit-step function. Therefore $\Xi(z,\Gamma)\to\theta(1-z)$ when $\Gamma\to 0$ and from Eq. (22) we find

$$S_{\rm ind}(\lambda) \simeq \frac{8Z^2\Sigma_0}{3\pi^2\chi^2}\lambda\int_0^1\frac{\mathcal{Z}^2(\alpha,z)z^3dz}{[z^2+\chi^2 f(z)]^2} = \frac{8Z^2\Sigma_0}{3\pi^2\chi^2}\lambda\mathcal{R}_{\rm ind}(\alpha,\chi^2). \tag{31}$$

For pointlike projectiles $[\mathcal{Z}(z,\alpha)\to 1]$ the last expression becomes the known result (see, e.g., Ref. [4]). These approximate analytical results are well supported by full numerical calculations. In Fig. 1 we show the friction coefficient $\mathcal{R}_{\rm ind}(\alpha,\Gamma,\chi^2)$ for He^+ ion ($Z=2$) vs damping parameter Γ for two values of the density parameter $r_s=2.677$ and $r_s=2.069$ corresponding to the valence electron densities in Cu and Al respectively. The lines with circles are for a proton projectile. As expected, the friction coefficient and hence the SP increase with an increasing damping parameter Γ; this was previously reported in Refs. [12–14].

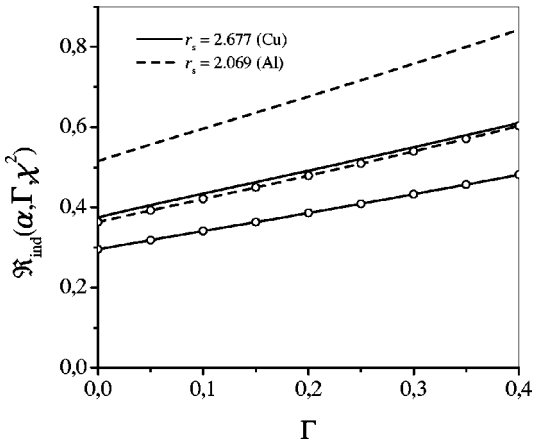

FIG. 1. The friction coefficient $\mathcal{R}_{\rm ind}(\alpha,\Gamma,\chi^2)$ for the He^+ ion ($Z=2$) vs damping parameter Γ for various materials. $r_s=2.677$ (solid lines), $r_s=2.069$ (dashed lines). The lines with circles are for the proton (pointlike) projectile.

The approximation (22) implies that the SP is proportional to velocity. The velocity region in which the linear proportionality between SP and the projectile velocity holds may be inferred from the numerical calculations (see Sec. IV) and the recent experimental results [25] on low-energy proton and antiproton energy losses. It is seen from those results that the approximation (22) remains quite accurate even when λ becomes as large as ~ 1.

B. Low-velocity limit: Extended ions ($\gamma=0$)

We shall now evaluate the last expression for ISP of extended ions. To evaluate Eq. (31) we split it into two parts as follows:

$$\mathcal{R}_{\rm ind}(\alpha,\chi^2) = L_1(\chi^2)+Z^{-2}\hat{\mathcal{Z}}(\alpha)L_2(\alpha,\chi^2), \tag{32}$$

where

$$L_1(\chi^2) = \int_0^1\frac{z^3dz}{[z^2+\chi^2 f(z)]^2}, \quad L_2(\alpha,\chi^2) = \int_0^1\frac{z^3dz}{(z^2+\alpha^2)[z^2+\chi^2 f(z)]^2}, \tag{33}$$

$$\hat{\mathcal{Z}}(\alpha) = \alpha^3\left[\left(Z-\frac{1}{16}\right)\frac{\partial}{\partial\alpha}+\frac{\alpha}{16}\frac{\partial^2}{\partial\alpha^2}-\frac{\alpha^2}{48}\frac{\partial^3}{\partial\alpha^3}\right]. \tag{34}$$

Here the differential operator $\hat{\mathcal{Z}}(\alpha)$ is as introduced in Refs. [18,19]. The first term in Eq. (32) is responsible for the energy loss of pointlike nucleus with charge Z. The second term describes the energy loss of an individual bound electron and the vicinage energy loss due to an interference interaction between pointlike nucleus and the bound electron with its spherically symmetric spatial distribution. We note that the functions $L_1(\chi^2)$ and $L_2(\alpha,\chi^2)$ can be approximated quite well by substituting for $f(z)$ the first two terms in a series expansion in powers of z^2, i.e., for $f(z)\simeq 1-z^2/3$. It then follows from Eq. (33) that

$$L_1(\chi^2) = \frac{1}{2(1-\chi^2/3)^2}\left[\ln\left(\frac{2}{3}+\frac{1}{\chi^2}\right) - \frac{1-\chi^2/3}{1+2\chi^2/3}\right], \quad (35)$$

$$L_2(\alpha,\chi^2) = \frac{1}{2[\alpha^2(1-\chi^2/3)-\chi^2]} \times\left[\frac{\alpha^2}{\alpha^2(1-\chi^2/3)-\chi^2}\ln\frac{\alpha^2(1+2\chi^2/3)}{\chi^2(1+\alpha^2)} - \frac{1}{1+2\chi^2/3}\right]. \quad (36)$$

Equation (35) was obtained by Lindhard and Winther [4]. For some further simplification of Eq. (36) we note that even for a light ion like He^+ and for a metallic target material, $\alpha = \pi\chi^2 Z \geqslant 2$. Thus the parameter α can be very large for heavy ions with $Z \gg 1$. Therefore from Eqs. (32), (33), (35), and (36), and using the equation

$$\hat{\mathcal{Z}}(\alpha)\left(\frac{1}{\alpha^l}\right) = \left[\frac{1}{16} - Z + \frac{(l+1)(l+5)}{48}\right]\frac{l}{\alpha^{l-2}} \quad (37)$$

for an arbitrary l, we finally find the following asymptotic expression (for large α):

$$\mathcal{R}_{\rm ind}(\alpha,\chi^2) \simeq q_1^2 L_1(\chi^2) + \Delta L(\alpha,\chi^2), \quad (38)$$

where

$$\Delta L(\alpha,\chi^2) = \frac{qq_1}{\alpha^2}\Delta L_1(\chi^2) - \frac{q(3-5q)}{\alpha^4}\Delta L_2(\chi^2), \quad (39)$$

$$\Delta L_1(\chi^2) = \frac{2}{(1-\chi^2/3)^2}\left[\frac{1+5\chi^2/3}{1+2\chi^2/3} - \frac{2\chi^2}{1-\chi^2/3}\ln\left(\frac{2}{3}+\frac{1}{\chi^2}\right)\right], \quad (40)$$

$$\Delta L_2(\chi^2) = \frac{1}{2(1-\chi^2/3)^3}\left[\frac{1-11\chi^2/3-44\chi^4/9}{1+2\chi^2/3} + \frac{6\chi^4}{1-\chi^2/3}\ln\left(\frac{2}{3}+\frac{1}{\chi^2}\right)\right]. \quad (41)$$

We have introduced the notations $q=1/Z$ and $q_1=1-q$. Now the coefficients $\Delta L_1(\chi^2)$ and $\Delta L_2(\chi^2)$ depend only on the target density. The accuracy of the derived asymptotic result is illustrated in Fig. 2 both for proton (dotted line) and extended He^+ ion (solid and dashed lines) projectiles, where the approximate expression for $\mathcal{R}_{\rm ind}(\alpha,\chi^2)$ is compared with the result of a numerical integration of Eq. (31). As seen from Fig. 2 both exact (solid line) and approximate (dashed line) data for $\mathcal{R}_{\rm ind}$ practically lie on the same curve. Also Fig. 2 shows an enhancement of the friction coefficient for extended ions. This is due to the effective charge for extended ions remaining higher than the projectile total charge, Z_t [see Eqs. (22) and (31)].

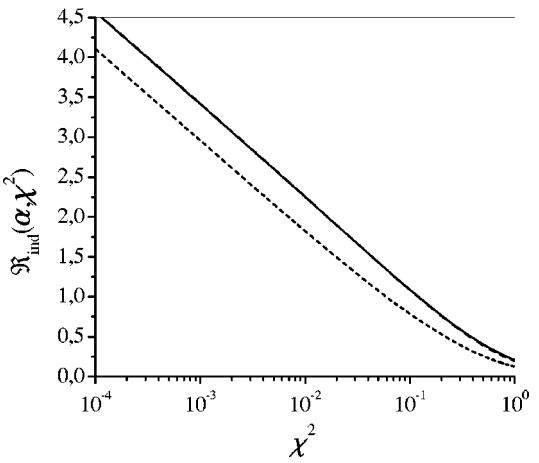

FIG. 2. The friction coefficient $\mathcal{R}_{\rm ind}(\alpha,\chi^2)$ [Eq. (31)] of the He^+ ion vs material density (χ^2). The solid and dashed lines correspond to exact and approximate expressions (31), (35), and (38)–(41), respectively. The dotted line corresponds to the proton projectile.

C. High-velocity limit: General formulation

Consider next the limit of large projectile velocities. In this limit the general expression (6) for poinlike projectiles with charge Z moving in a DEG without damping ($\gamma=0$) reduces to the simple Bethe-Bohr formula [4],

$$S_{\rm BB} = \frac{8\Sigma_0 Z^2}{3\pi^2\chi^2\lambda^2}\ln\left(\frac{\sqrt{3}}{\chi}\lambda^2\right) = \frac{Z^2e^2\omega_p^2}{v^2}\ln\left(\frac{2mv^2}{\hbar\omega_p}\right). \quad (42)$$

In the presence of damping and for extended ions this formula is shown to be significantly modified. We derive below a generalized expression for SP, in a high-velocity limit, for extended ions moving in a disordered ($\gamma=0$) DEG. Only ISP in a high-velocity limit is considered. In order to show how ISP in a high-velocity limit is affected we consider the stopping number of an extended projectile, $L(\alpha,\lambda)$, which relates to ISP as follows:

$$S_{\rm ind}(\lambda) = \frac{8Z^2\Sigma_0}{3\pi^2\chi^2\lambda^2}L(\alpha,\lambda), \quad (43)$$

$$L(\alpha,\lambda) = \frac{6}{\pi\chi^2}\int_0^\lambda \frac{du}{u}\Lambda(\alpha,u), \quad (44)$$

where

$$\Lambda(\alpha,u) = u^2\int_0^\infty \mathcal{Z}^2(\alpha,z)\,{\rm Im}\frac{-1}{\varepsilon(z,u,\Gamma)}z\,dz = \Lambda_0(u) + Z^{-2}\hat{\mathcal{Z}}(\alpha)\Lambda_1(\alpha,u), \quad (45)$$

$$\Lambda_0(u) = u^2\int_0^\infty {\rm Im}\frac{-1}{\varepsilon(z,u,\Gamma)}z\,dz, \quad (46)$$

$$\Lambda_1(\alpha,u) = u^2\int_0^\infty {\rm Im}\frac{-1}{\varepsilon(z,u,\Gamma)}\frac{z\,dz}{z^2+\alpha^2}. \quad (47)$$

In Eq. (45) the first term is the SP of projectile pointlike nucleus and the second term is responsible to the energy loss by individual bound electron and the interference effect.

The expression (44) can be written in the equivalent form

$$L(\alpha,\lambda) = L_0 + \frac{6}{\pi\chi^2}[\Lambda_\infty \ln\lambda - l(\alpha,\lambda)], \tag{48}$$

where $\Lambda_\infty = \Lambda(\alpha, u\to\infty)$,

$$L_0 = \frac{6}{\pi\chi^2}\left\{\int_0^1 \frac{du}{u}\Lambda(\alpha,u) + \int_1^\infty \frac{du}{u}[\Lambda(\alpha,u) - \Lambda_\infty]\right\}, \tag{49}$$

$$l(\alpha,\lambda) = \int_\lambda^\infty \frac{du}{u}[\Lambda(\alpha,u) - \Lambda_\infty]. \tag{50}$$

The first two terms in Eq. (48) give the leading logarithmic term in the case of an extended ion moving in a disordered DEG. The second term inside the square brackets in Eq. (48) gives a high-velocity correction to the main logarithmic contribution. This requires an evaluation of $l(\alpha,\lambda)$ at $\lambda \gg 1$ and hence we need to derive an asymptotic expression for $\Lambda(\alpha,u)$ at large u. The evaluation of the functions $\Lambda_0(u)$ and $\Lambda(\alpha,u)$ is done in detail in Appendix A.

Using the parameters q and q_1, the asymptotic expansion for $\Lambda(\alpha,u)$ then finally reads (see Appendix A for more details)

$$\Lambda(\alpha,u) = \frac{\pi\chi^2}{3}\left\{C_0 + \frac{C_1}{2u} + \frac{C_2}{u^2} + \frac{3C_3}{2u^3} + \frac{2C_4}{u^4} + \cdots\right\}, \tag{51}$$

where

$$C_0 = \frac{1+q_1^2}{2}, \quad C_1 = \frac{\Gamma q}{\alpha}\left(3 - \frac{35}{16}q\right), \tag{52}$$

$$C_2 = \frac{3(1+q_1^2)}{10} + \frac{2qq_1}{\alpha^2}\left(\frac{\chi^2}{3} - \Gamma^2\right) - \frac{12q_1^2\Gamma^4}{5\chi^4}, \tag{53}$$

$$C_3 = \frac{2\Gamma q}{3}\left\{\frac{9}{10\alpha}\left(3 - \frac{35q}{16}\right) - \frac{3\alpha}{2}\left(1 - \frac{5q}{16}\right) - \frac{5(3\Gamma^2 - 2\chi^2)}{6\alpha^3}\left(\frac{21q}{16} - 1\right) - \frac{4}{3\pi\alpha^2}\left[\frac{5q-3}{\alpha^2} + \frac{7(16-33q)}{24\pi\alpha^3} + 2q_1\right]\right\}, \tag{54}$$

$$C_4 = \frac{1+q_1^2}{2}\left(\frac{3}{14} + \frac{\chi^2}{3}\right) + \frac{2q_1^2\Gamma^2}{7}\left[\frac{27\Gamma^2}{5\chi^4}\left(\frac{\Gamma^4}{5\chi^4} - 3\right) + \frac{14\Gamma^4}{\chi^4}\left(1 + \frac{24}{25\chi^2}\right) - \frac{119}{12}\right] - \frac{3\Gamma^2 q(2-q)}{2} + \frac{q(5q-3)}{2\alpha^4}\left(\frac{\chi^4}{9} + \Gamma^4 - \Gamma^2\chi^2\right) - \frac{q\alpha^4}{2} + \frac{2qq_1}{\alpha^2}\left[\frac{\chi^2}{5} + \frac{33\Gamma^2}{20} - \frac{12\Gamma^4}{5\chi^4}\left(\frac{\chi^2}{3} - \frac{\Gamma^2}{2}\right) + \frac{\Gamma^2}{\chi^2/3 - \Gamma^2/4}\left(\frac{\Gamma^4}{5\chi^2} + \frac{211\Gamma^2}{240} - \frac{49\chi^2}{60} - \frac{3\Gamma^6}{10\chi^4}\right)\right] - \frac{\Gamma^2 q}{16\pi\alpha^3}\left[5(16-21q) + \frac{7}{\alpha^2}(33q-16)\right]. \tag{55}$$

Note that asymptotic expansion (51) is valid for the values $u > \alpha$. Also in order to arrive at Eqs. (51)–(55) we again assumed that $\alpha > 2$ for a realistic medium and for extended ions, and used the following approximate expressions:

$$\hat{\mathcal{Z}}(\alpha)\frac{1}{\alpha^5[S_R^{(0)}(\alpha) - 1]} \simeq \frac{8}{\pi\chi^2\alpha^2}\left(2Z_t - \frac{3Z_t - 2}{\alpha^2}\right), \tag{56}$$

$$\hat{\mathcal{Z}}(\alpha)\frac{1}{\alpha^6[S_R^{(0)}(\alpha) - 1]} \simeq \frac{20}{\pi\chi^2\alpha^3}\left(Z_t - \frac{5}{16}\right). \tag{57}$$

From Eqs. (51) and (52) we find that

$$\Lambda_\infty = \frac{\pi\chi^2}{6}(1+q_1^2). \tag{58}$$

Now we can calculate the function $l(\alpha,\lambda)$ at high-velocity limit. From Eqs. (50), (51), and (58) we find for $\lambda > \alpha$ (or $v > Zv_0 = Ze^2/\hbar$)

$$l(\alpha,\lambda) = \frac{\pi\chi^2}{6}\left(\frac{C_1}{\lambda} + \frac{C_2}{\lambda^2} + \frac{C_3}{\lambda^3} + \frac{C_4}{\lambda^4} + \cdots\right). \tag{59}$$

Let us consider some particular cases for the expansion coefficients C_0, C_1, C_2, C_3, and C_4. For a pointlike projectile moving in a disordered DEG at the limit $Z\to\infty$ we find from Eqs. (52)–(55)

$$C_0 = 1, \quad C_1 = C_3 = 0, \quad C_2 = \frac{3}{5} - \frac{12\Gamma^4}{5\chi^4}, \tag{60}$$

$$C_4 = \frac{3}{4} + \frac{\chi^2}{3} + \frac{2\Gamma^2}{7}\left[\frac{27\Gamma^2}{5\chi^4}\left(\frac{\Gamma^4}{5\chi^4} - 3\right) + \frac{14\Gamma^4}{\chi^4}\left(1 + \frac{24}{25\chi^2}\right) - \frac{119}{12}\right].$$

In another case when an extended ion moves in a damping-free medium ($\Gamma = 0$) we obtain from Eqs. (52)–(55)

$$C_0 = \frac{1+q_1^2}{2}, \quad C_1 = C_3 = 0, \quad C_2 = \frac{2qq_1\chi^2}{3\alpha^2} + \frac{3(1+q_1^2)}{10}, \tag{61}$$

$$C_4 = \frac{1+q_1^2}{2}\left(\frac{3}{14} + \frac{\chi^2}{3}\right) + \frac{2qq_1\chi^2}{5\alpha^2} + \frac{\chi^4 q(5q-3)}{18\alpha^4} - \frac{q\alpha^4}{2}.$$

For a pointlike projectile moving in a DEG without damping both Eqs. (60) and (61) lead to the known result (see, e.g., Ref. [4])

$$C_0 = 1, \quad C_1 = C_3 = 0, \quad C_2 = \frac{3}{5}, \quad C_4 = \frac{3}{14} + \frac{\chi^2}{3}. \tag{62}$$

The calculation of L_0 merits a separate presentation and is done in detail in Appendix B. From Eqs. (48), (58), (59), and (B7), for stopping number $L(\alpha,\lambda)$ we finally find

$$L(\alpha,\lambda) = q_1^2 \ln\left[\frac{\sigma_2\sqrt{3}}{\chi\alpha^{\sigma_1}} e^{-Q(\eta)}\lambda^{2+\sigma_1}\right] - \frac{C_1}{\lambda} - \frac{C_2}{\lambda^2} - \frac{C_3}{\lambda^3} - \frac{C_4}{\lambda^4} - \cdots, \tag{63}$$

where σ_1 and σ_2 are given by Eq. (B2). The function $Q(\eta)$ is given by Eq. (B2) and depends on damping parameter Γ through relation $\eta=\Gamma\sqrt{3}/2\chi$ (see Appendix B) and has been obtained under the assumption that $\gamma<2\omega_p$. When the damping vanishes ($\Gamma\to 0$). this function $Q(\eta)\to 0$. The function $Q(\eta)$ increases with the damping parameter Γ and at $\eta=1$, $Q(\eta)=1$.

For a pointlike projectile ($\sigma_1=0$, $\sigma_2=1$) but for nonzero damping from Eq. (63) we obtain

$$L(\alpha,\lambda) = \ln\left[\frac{2m\upsilon^2}{\hbar\bar{\omega}(\Gamma)}\right] - \frac{C_2}{\lambda^2} - \frac{C_4}{\lambda^4} - \cdots, \tag{64}$$

where $\bar{\omega}(\Gamma)=\omega_p e^{Q(\eta)}$. So, the leading logarithmic term in the stopping number depends on the target conditions through the electron density and the parameter Γ. The coefficients C_2 and C_4 are defined as in Eq. (60). Equation (64) is the modified Bethe-Bohr SP formula with the excitation energy $\hbar\bar{\omega}(\Gamma)$ which now depends on the damping parameter Γ. It increases monotonically with an increasing damping parameter Γ.

To make contact with an experimental situation in which a carbon foil is used, we choose values of the parameters corresponding to the valence electrons in carbon. With four electrons per atom the density and damping parameters are $r_s=1.6$ and $\hbar\gamma=15$ eV (or $\Gamma=0.19$), respectively. For this values we find that $\bar{\omega}(\Gamma)=1.52\omega_p$ and the damping effect can give an observable effect for projectile intermediate velocity range.

Consider now an extended ion moving damping-free electron gas ($\Gamma=0$). From Eq. (63)

$$L(\alpha,\lambda) = q_1^2 \ln\left[\frac{2m\upsilon^2}{\hbar\omega_p}\sigma_2\left(\frac{\upsilon}{Z\upsilon_0}\right)^{\sigma_1}\right] - \frac{C_2}{\lambda^2} - \frac{C_4}{\lambda^4} - \cdots, \tag{65}$$

where the coefficients C_2 and C_4 are given by Eq. (61). Here the parameters σ_1 and σ_2 depend only the projectile nuclear charge Z [see Appendix B, Eq. (B2)] and hence from Eq. (65) it is now seen that the leading logarithmic term depends also on an extended ion property through the parameter Z.

For a pointlike projectile and from Eq. (65) in the limit $\sigma_1\to 0$ and $\sigma_2\to 1$ we obtain the Bethe-Bohr logarithmic stopping number $\ln(2m\upsilon^2/\hbar\omega_p)$ [see Eq. (42)]. Therefore the Bethe-Bohr SP asymptotic formula is significantly modified both for extended ions and due to the presence of damping. Now the logarithmic term depends on $\upsilon^{2+\sigma_1}$ which may be contrasted with the usual quadratic, i.e., υ^2 dependence. For light He^+ ($Z=2$), Li^{2+} ($Z=3$), and Be^{3+} ($Z=4$) ions, for instance, $\sigma_1=3$, $\sigma_2\simeq 3$, $\sigma_1=1.25$, $\sigma_2\simeq 1.68$, and $\sigma_1=7/9\simeq 0.77$, $\sigma_2\simeq 1.4$, respectively. Then for the logarithmic SP we find $\ln[0.375U(\upsilon/\upsilon_0)^5]$, $4\ln[0.425U(\upsilon/\upsilon_0)^{3.25}]$, and $9\ln[0.481U(\upsilon/\upsilon_0)^{2.77}]$, respectively, where the function $U=\pi^2\chi^3\sqrt{3}e^{-Q(\eta)}$ depends on the target parameters χ and Γ.However, for heavy ions with $Z\gg 1$ the dependence of the logarithmic term in Eq. (63) on Z becomes less important and the stopping number is similar to the Bethe-Bohr expression. Then an enhancement of the SP is caused due to the usual quadratic dependence, $Z_t^2\sim Z^2$ in Eqs. (42) and (43). Let us note, however, that for heavy ions the nonlinear coupling between the projectile and the target may play an important role [6] and Eq. (63) then breaks down.

D. Asymptotic ($N\to\infty$) SP of N-ion chain

It is of interest to consider the asymptotic ($N\to\infty$) limit of the SP of an N-ion chain.

From Eqs. (20) and (21) and using the mathematical relation

$$\frac{1}{\pi N}\left[\frac{\sin(Nx)}{\sin(x)}\right]^2\Bigg|_{N\to\infty} = \sum_{n=-\infty}^{\infty}\delta(x-\pi n) \tag{66}$$

we find

$$K(\lambda,R) = \frac{S_N}{N}\Bigg|_{N\to\infty} = 16\pi Z^2\Sigma_0\left(\frac{a_0}{R}\right)^2\sum_{n=1}^{\infty} n\int_0^1 \mathcal{Z}^2(\alpha,\zeta_n/u) \times \mathrm{Im}\frac{-1}{\varepsilon(\zeta_n/u,\lambda u,\Gamma)}\frac{du}{u}, \tag{67}$$

where $\zeta_n=\pi n/\xi$ ($\xi=k_F R$). Equation (67) shows that for a high N-ion chain, with the ions not necessarily uniformly distributed along the chain, SP is linearly proportional to the number N of ions: $S_N=K(\lambda,R)N$, where $K(\lambda,R)$ depends on the target density γ and the individual ion structure factor. One can find close analytical expressions for S_N in some particular cases. Before presenting these results we note some limiting values of the SP with respect to R. Recalling the exact RPA expression for the N-ion chain SP [see Eq. (20)] we see that R enters only in the chain structure factor, i.e., the quantity in square brackets in Eq. (21). In the usual units $zu\xi/\lambda=\omega R/2\upsilon$. Then the SP depends on R through the combination RN which is a measure of the size of the ensemble of ions in the chain. Because of this combination it is seen that in the exact and also in the asymptotic expressions for the SP at $N\gg 1$, R can be arbitrarily large but not arbitrarily small. This can be understood if the one-dimensional chain of N ions is viewed as a lattice and not as a continuum of charges. An estimate of this minimum interionic separation length $R_{\min}$ can be made from the following physical considerations. In a velocity limit $\upsilon\sim\upsilon_F$ such that the linear response theory can still be valid $R_{\min}$ may be estimated from the argument of the sinus function in Eq. (21), which involves $N\omega R/2\upsilon$. For ($N\to\infty$), it is sufficient to assume that $R>\upsilon/\omega$ implying a minimum length $R_{\min}\cong\upsilon/\omega$, where the frequency ω corresponds to either the collective or single-particle excitations. For smaller velocities $\upsilon<\upsilon_F$ not invalidating the linear response theory, $R_{\min}$ is of the order of the Thomas-Fermi screening length.

As we discussed in Sec. II B the per SP ion of N-ion chain, S_N/N, becomes the individual SP of an ion for large interionic distances R. This result can be recovered from Eq. (67) if the sum in $R\to\infty$ limit is replaced by an integral over

the variable $\zeta_n/u=\pi n/u\xi\to z$ which gives again $K(\lambda,R\to\infty)=S_{\rm ind}(\lambda)$.

1. Low-velocity limit

In a low-velocity limit when $v\ll v_F$, the linear response theory of SP is still valid provided the projectile ions are of a low ionization level, e.g., for singly charged ions like H^+, He^+, and Be^+, etc. (For highly charged ions when the total projectile charge in a chain is quite high, the linear response theory may not be valid in a low-velocity limit.) In this limit Eq. (67) can be replaced by

$$K(\lambda,R)\simeq 8\pi^5\chi^6Z^2\Sigma_0\frac{v}{v_0}\left(\frac{a_0}{R}\right)^3\sum_{n=1}^{\infty}n^2\int_{\zeta_n}^{\infty}\frac{\mathcal{Z}^2(\alpha,z)\Xi(z,\Gamma)dz}{[z^2+\chi^2f(z)]^2} \tag{68}$$

with the quantities introduced earlier. For a further analytical manipulation of Eq. (68) let us consider the case of vanishing damping but for an extended projectile. In this limit $\Xi(z,\Gamma)=\theta(1-z)$ [(cf. Eq. (30)], where $\theta(z)$ is the Heaviside unit-step function. It then follows from Eq. (68) that $S_N/N=0$ for $0\leqslant\rho\leqslant 1$ where $\rho=k_FR/\pi$. The last result indicates that Eq. (68) is not valid for $\gamma=0$ (i.e., for a disorder-free DEG) when R is small such that $R<\pi/k_F=R_{\rm min}$. For $\rho>1$ and for $\gamma=0$, Eq. (68) can be expressed as

$$K(\lambda,R)=8\pi^5\chi^2Z^2\Sigma_0\frac{v}{v_0}\left(\frac{a_0}{R}\right)^3\sum_{n=1}^{n_1}n^2\Theta\left(\frac{n}{\rho}\right). \tag{69}$$

Here n_1 stands for $E[\rho]$, where $E[\rho]$ denotes the integer part of ρ, and

$$\Theta(s)=\chi^4\int_s^1\frac{\mathcal{Z}^2(\alpha,z)dz}{[z^2+\chi^2f(z)]^2}. \tag{70}$$

The function $\Theta(s)$ can be approximated quite well by substituting for $f(z)$ the first two terms in a series expansion in powers of z^2, i.e., for $f(z)\simeq 1-z^2/3$ (see Sec. III B). For further simplification of Eqs. (69) and (70) we note that even for a light ion like He^+ and for a metallic target material, $\alpha=\pi\chi^2Z\geqslant 2$. Thus the parameter α can be very large for the heavy ions with $Z\gg 1$. It then follows from Eq. (70) that

$$\Theta(s)\cong d^2q_1\left(\frac{q_1}{2}-\frac{2qd^2}{\alpha^2}\right)\left(\frac{1}{d^2+1}-\frac{s}{d^2+s^2}\right)+dq_1\left(\frac{q_1}{2}+\frac{2qd^2}{\alpha^2}\right)\left(\arctan\frac{1}{d}-\arctan\frac{s}{d}\right), \tag{71}$$

where $d=\chi/\sqrt{1-\chi^2/3}$. The numerical calculations show that the relative difference of exact [Eqs. (69) and (70)] and approximate [Eqs. (69) and (71)] expressions is less than 1 % for metallic densities.

2. High-velocity limit

In the high velocity limit the simple plasmon-pole approximation (PPA) for the linear response function with the plasmon dispersion is widely used (see, e.g., Refs. [7,20,21]). Here we consider the high-velocity limit of the N-ion chain SP for vanishing damping. Within PPA and for $\gamma\to 0$ using the variables z and u we present the imaginary part of $1/\varepsilon(z,u,\Gamma)$ in the following form [20]:

$$\mathrm{Im}\frac{-1}{\varepsilon(z,u,\Gamma)}=\frac{\pi\chi^2}{6uz}\delta\left(uz-\sqrt{\frac{\chi^2}{3}+\frac{3}{5}z^2+z^4}\right). \tag{72}$$

The argument of the Dirac δ function in Eq. (72) gives the dispersion relation between ω and k. In the usual units this relation becomes $\omega^2_{\rm PPA}(k)=\omega_p^2+(3/5)k^2v_F^2+\hbar^2k^4/4m^2$.

Substitution of Eq. (72) into Eq. (67) gives the expression (C1) (see Appendix C for details). For a further simplification of Eq. (C1) we assume that (i)$\delta=\rho/\lambda=(\sqrt{3}/\chi)\times(R/\lambda_P)<1$, where $\lambda_P=2\pi v/\omega_P$ is the plasmon wavelength or $R<\lambda_P$ (long-wavelength limit), (ii) $\lambda\gg\max[1;1/\rho;\alpha]$. The second condition, $\lambda\gg 1/\rho$, gives for an ion with a given velocity v, the value $R_{\rm min}\simeq\pi\lambda_{DB}$, where $\lambda_{DB}=\hbar/mv$ is the de Broglie wavelength of a target electron. The third condition, $\lambda\gg\alpha$, is equivalent to the condition $v\gg Ze^2/\hbar$ of the first Born approximation, which is valid here only for light projectile ions. In this limit we find $n_1=1$, $n_2\cong E|\lambda\rho|\gg 1$, and Eq. (C1) yields (see Appendix C for details)

$$K(\lambda,R)\cong\frac{4Z^2\Sigma_0}{3\pi^2\chi^2\lambda^2}\left\{\ln(\gamma_1\lambda\rho)+\frac{1}{2\lambda}\left(\frac{1}{\rho}+\frac{\pi^2\rho}{10}\right)+\frac{1}{\lambda^2}\left[\rho^2\zeta(3)\times\left(\frac{\chi^2}{3}-2q\alpha^4\right)-\frac{3}{5}-\frac{1}{12\rho^2}\right]\right\}. \tag{73}$$

Here $\zeta(z)$ is the Riemann zeta function with $\zeta(3)\cong 1.202$, $\gamma_1=e^C=1.781$, and $C=0.5772$ is the Euler's constant.

IV. NUMERICAL RESULTS AND DISCUSSION

Using the theoretical results obtained in Secs. II and III, we present here detailed numerical calculations of stopping power and related quantities for a target material with the density parameter $r_s=2.07$ corresponding to the valence electron density in Al. The target material is modelled as an electron gas whose linear response function, within RTA, is given by Eqs. (9)–(14) with γ as a model damping parameter. In Figs. 3–5 and 6(a) based on numerical calculations we choose four values of γ:$\hbar\gamma=0$ (solid lines), $\hbar\gamma=3$ eV (dashed lines), $\hbar\gamma=10$ eV (dash-dotted lines), and $\hbar\gamma=15$ eV (dotted lines). The values $0<\hbar\gamma<3$ eV are comparable with the damping parameters (related inversely to the collision times) in some metal targets, e.g., Al for which $\hbar\gamma$ can be $\sim$0.1 eV. The last value $\hbar\gamma=15$ eV corresponds to the damping parameter in carbon [12–14].

As examples of ion beams we have considered three types of projectiles: (i) individual He^+ ion, (ii) He^+ ion dicluster, and (iii) N–He^+ ion chain with the orientation angle $\vartheta=0$. For case (ii) we choose two values, 0 and $\pi/2$, for the di-He^+ ion cluster orientation angle ϑ. Correlations between two He^+ ions in the dicluster are maximum and minimum, respectively, for these two values of ϑ. For high-velocity projectiles it is useful to introduce the wavelength $\lambda_p=2\pi v/\omega_p$ which can be expressed by the density and velocity parameters r_s and λ, respectively, $\lambda_P=3.683r_s^{1/2}\lambda$ (in Å). The velocity parameter is $\lambda=0.52r_sv/v_0$. For the value r_s

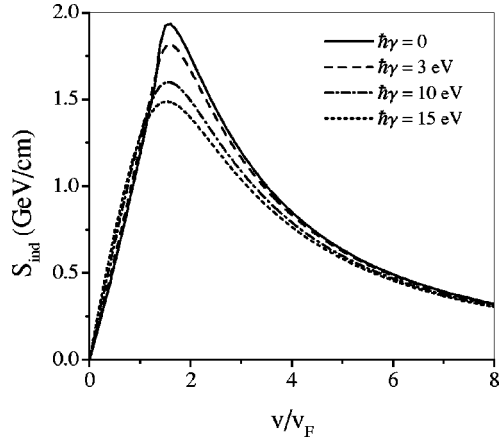

FIG. 3. ISP of an individual He^+ ion vs v/v_F for $r_s=2.07$. $\gamma=0$ (solid line), $\hbar\gamma=3$ eV (dashed line), $\hbar\gamma=10$ eV (dash-dotted line), $\hbar\gamma=15$ eV (dotted line).

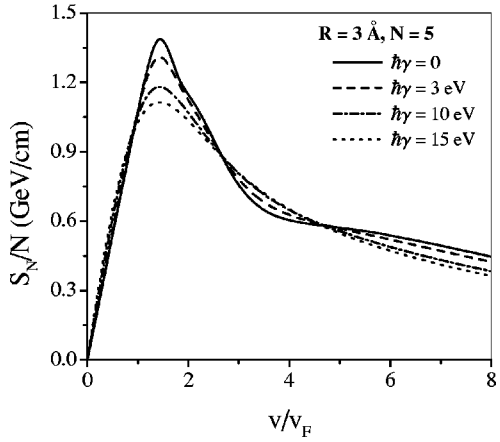

FIG. 5. S_N/N of an N-helium linear chain with $R=3$ Å and $N=5$ vs v/v_F for $r_s=2.07$. $\gamma=0$ (solid line), $\hbar\gamma=3$ eV (dashed line), $\hbar\gamma=10$ eV (dash-dotted line), $\hbar\gamma=15$ eV (dotted line).

$=2.07$ one finds $\lambda_p=5.31\lambda$ (in Å) and $\lambda=1.08v/v_0$.

For projectiles (i) and (ii) we present theoretical results for the stopping power $S/2$, vicinage function g, together with the dependence of $S/2$ and g on R, the interionic separation distance within the cluster. As in our previous paper [7], SP has been divided by a factor of 2. The reason, as discussed in Sec. II A, is that the SP results for a di-He^+ ion cluster are expected to reduce asymptotically (as R tends to infinity) to those for two uncorrelated ions, the latter being referred to as individual SP ISP. The SP for the projectile (iii) S_N has been treated in the same way.

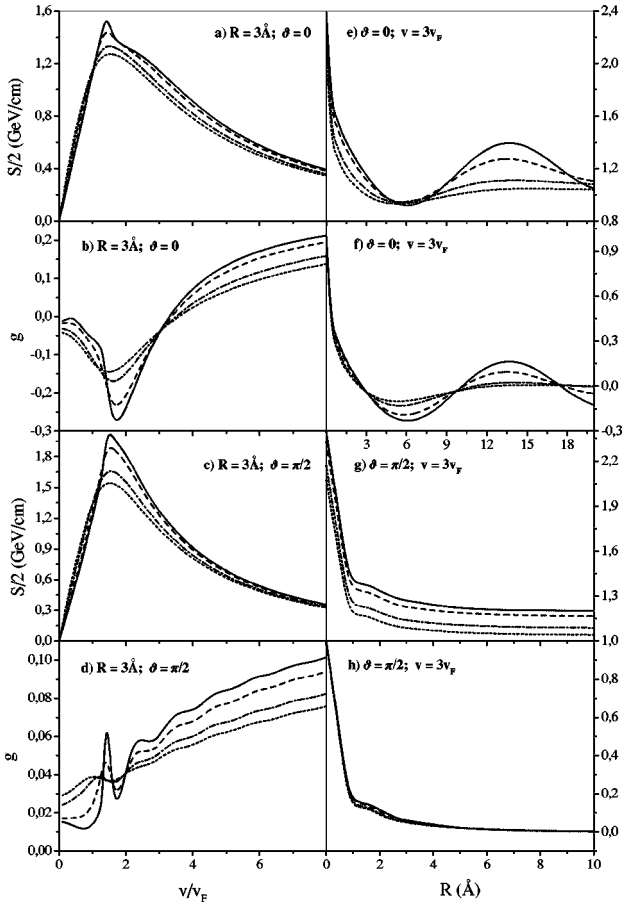

FIG. 4. $S/2$ and g of a di-helium cluster vs v/v_F (left column) and R (right column) with (a) and (b) $R=3$ Å and $\vartheta=0$; (c) and (d) $R=3$ Å and $\vartheta=\pi/2$; (e) and (f) $v=3v_F$ and $\vartheta=0$; (g) and (h) $v=3v_F$ and $\vartheta=\pi/2$. $r_s=2.07$, $\gamma=0$ (solid line), $\hbar\gamma=3$ eV (dashed line), $\hbar\gamma=10$ eV (dash-dotted line), $\hbar\gamma=15$ eV (dotted line).

Figure 3 shows ISP while Fig. 4 shows di-He^+ ion cluster SP and vicinage function (VF) as a function of v/v_F and R for the two above-mentioned values of ϑ. In a low-velocity limit these figures show an enhancement of the SP with an increasing damping parameter γ. The numerical calculation of the friction coefficient shows this result more clearly (see Fig. 1). As discussed in Sec. I, this is due to the broadening of the plasmon peak with increasing γ which shifts the threshold for the energy loss by plasmon excitation towards lower projectile velocities. These results have been reported previously [12]. However, in a high-velocity limit the damping decreases the energy loss rate (see Figs. 3 and 4) and this is shown explicitly by the logarithmic term in Eq. (63). The numerical calculations of the last expression for ISP in a high-velocity limit show that the asymptotic curves coincide with the exact ones [based on Eqs. (9)–(14)] beginning with $\lambda\sim 2$. Hence it can be a good approximation for analyzing the experimental data on beam-target interactions.

Consider now the angular dependence of SP. It is seen from Figs. 4(a)–4(d) that in a medium velocity range ($v<4v_F$), SP has a remarkably higher value for the larger value of ϑ. This is likely due to single-particle excitations in this velocity range. In the higher velocity range, the dicluster wake field excitations become important and we find that the situation is reverse in the higher velocity range ($v>4v_F$) for which SP for $\vartheta=0$ is slightly larger than for $\vartheta=\pi/2$.

The interplay of correlations between the two ions and of damping can be explored by the plots in Figs. 4(b) and 4(d). Correlation effects are expected to be maximum when the two ions are aligned with each other in the direction of propagation of the dicluster motion ($\vartheta=0$) while they decay when ϑ tends to $\pi/2$, the latter behavior being related to the wake field due to the leading ion. For a chosen value of the

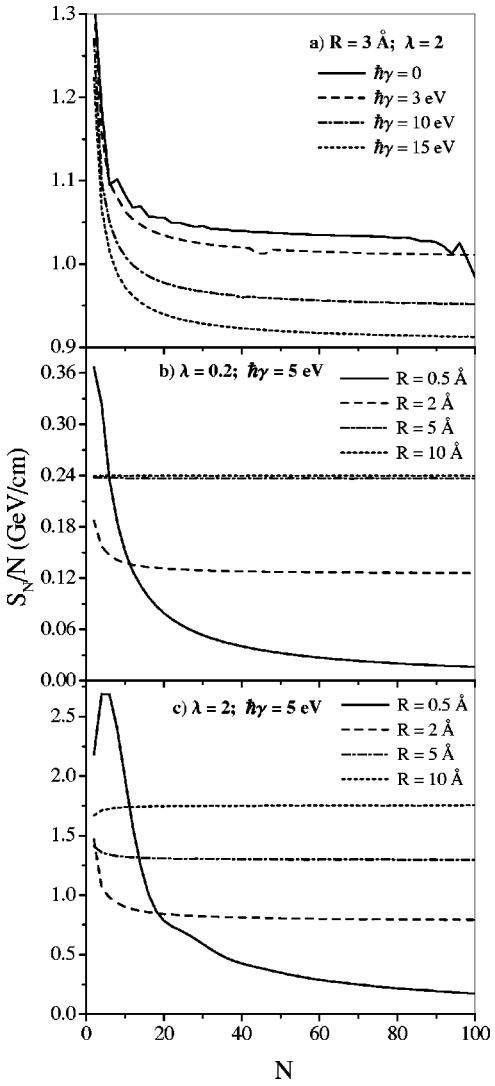

FIG. 6. S_N/N of an N-helium linear chain vs N for $r_s=2.07$ with (a) $R=3$ Å and $\lambda=2$, $\gamma=0$ (solid line), $\hbar\gamma=3$ eV (dashed line), $\hbar\gamma=10$ eV (dash-dotted line), $\hbar\gamma=15$ eV (dotted line); (b) $\lambda=0.2$ and (c) $\lambda=2$ with $\hbar\gamma=5$ eV, $R=0.5$ Å (solid line), $R=2$ Å (dashed line), $R=5$ Å (dash-dotted line), $R=10$ Å (dotted line).

interionic distance R, the vicinage function is negative at $v<4v_F$ for an aligned dicluster but it is positive in all velocity ranges for $\vartheta=\pi/2$. In the first case the correlation effects decrease the full SP and this is shown in Fig. 4(a) by the formation of a short plateau on the SP curve near the value $\lambda\sim 2$. As to the role of damping, it considerably softens the correlation effects for both values of ϑ at $v>v_F$.

We have so far plotted SP (divided by a factor 2) or VF vs the beam velocity v/v_F, for some fixed value of the interionic distance $R=3$ Å. We now look for some complementary information about SP, and plot SP as a function of R with a given value of $v=3v_F$. The objective is then to see how, for the maximum and minimum angular configurations, SP and VF depend on R and v/v_F. Figures 4(e)–4(h) show SP and VF for a di-He^+ ion cluster, for $\vartheta=0$ and $\vartheta=\pi/2$. These figures show an oscillatory character of SP and VF with respect to R. The oscillations are the highest for $\vartheta=0$ and lowest for $\vartheta=\pi/2$. It is seen from Figs. 4(e) and 4(f) that the oscillation wavelength in the longitudinal direction is about $\lambda_p=5.31\lambda\simeq 16$ Å for $\gamma=0$, while in the perpendicular direction [see Figs. 4(g) and 4(h)] the characteristic length scale $\lambda_\perp \ll \lambda_p$ and is not so sensitive to a variation of the damping parameter $\hbar\gamma$, as shown in Ref. [19]. It is noteworthy that in accordance to Ref. [19] the wavelengths of oscillations $\lambda_p=2\pi v/\omega_p$ at $\vartheta=0$ {see Figs. 4(e) and 4(f)] increase with $\hbar\gamma$ because the plasmon energy becomes smaller $\lambda\omega_p\to\hbar(\omega_p^2-\gamma^2/4)^{1/2}$. But the amplitudes are now weaker due to the collisional damping of plasmons. Let us note that the SP's in Figs. 4(e) and 4(g) tend asymptotically to the values of $S_{\rm ind}(\lambda)$ at $\lambda=3$ and $R\to\infty$ while at small $R\to 0$ the values of $S/2$ become $S_{\rm ind}(\lambda)$.

Having discussed SP's for a di-He^+ ion cluster, we now present results for the projectile type (iii), i.e., the quantity S_N/N for an $N-He^+$ ion chain with the orientation angle $\vartheta=0$. Figure 5 shows S_N/N vs v/v_F while Fig. 6 shows S_N/N vs ion number N at fixed R and λ [Fig. 6(a)], and at fixed λ and λ [Figs. 6(b) and 6(c)]. Figure 5 may be compared with Figs. 3 and 4(a). There are similarities but also some interesting differences, the latter being due to a multi-ion interference effect. We note that the interference effect between $N=5$ ions decreases the strength of SP per particle except in an extreme high-velocity limit $\lambda_p \gg (N-1)R$, where $(N-1)R$ is the total length of the N-ion cluster chain. In this limit the N-ion chain can be regarded as single entity and hence $S_N/N\sim NS_{\rm ind}(\lambda)\gg S_{\rm ind}(\lambda)$ [see, e.g., Eqs. (20) and (21)].

Next we present Fig 6. For a more detailed presentation we show the different plots in the same graph. It is clearly seen from this figure the asymptotic regime of the SP when the ion number N becomes very large. The SP per particle is saturated rapidly with increasing N. This regime has been investigated analytically in Sec. III D [see Eq. (67)]. Here again the collisional damping of the plasmons decreases the values of SPS [Fig. 6(a)]. Figures 6(b) and 6(c) show the SP in low- and high-velocity limits, respectively. The numerical data presented in these figures are well described by the analytical results given by Eqs. (68)–(71) (low velocities) and Eq. (73) (high velocities). As discussed in Sec. III D, the curves saturated rapidly rather for large interionic distances than for small one. It should be noted that the sawtooth profile of S_N/N vs N obtained within simple PPA (see Ref. [1]) is now replaced by the smooth curves in Fig. 6.

V. SUMMARY AND CONCLUDING REMARKS

In this paper we have presented a detailed theoretical study of the stopping power of point ion, extended ion, ion-cluster, as well as N-ion linear cluster projectiles in a degenerate electron gas containing disorder. In the course of this study we have also derived some analytical results for the disorder-inclusive RPA linear response function and for the corresponding plasmon dispersion relations. These analytical results go beyond those obtained in our previous paper [19]. After a general introduction to SP of a cluster of two and $N(N\geqslant 3)$ extended ions, in Sec. II, theoretical calculations of SP based on the linear response theory and using RTA are discussed in Sec. III. A number of limiting and asymptotic

regimes of low and high-velocities, large ion number N and vanishing damping have been studied. These approximate expressions are well supported by our numerical calculations. To our knowledge this is the most comprehensive study of the SP-related physical quantities using RTA in the linear response function. The theoretical expressions for a number of physical quantities derived in this section lead to a detailed presentation, in Sec. IV, of a collection of data through figures on individual (i.e., single-ion) and correlated stopping powers, vicinage function, of a single ion He^+ ion, di-He^+ and N-He^+ cluster projectiles for the target with density parameter $r_s=2.07$ corresponding to the valence electron density in Al. For the damping parameter, we have chosen a wide range of values $0 \leqslant \hbar\lambda \leqslant 15$ eV; the damping parameters (which are inversely related to the collision times) for some metal and semiconductor targets fall within this range. The results we have presented demonstrate that with regard to several physical quantities of primary interest the difference between RTA and usual RPA without damping is substantial while for others, specially for angular averaged quantities, this difference may not be of practical significance.

It is of particular interest to study the high-velocity limit for the SP of an ion beam. Such asymptotic expressions contain some useful information on a projectile ion structure factor and specially on the target medium properties. Equation (43) with Eq. (63) which are a generalization of the Bethe-Bohr asymptotic formula [4] can be used for analyses of experimental data on high-energy beam-target interactions.[1] We note that the analytical method developed here for the derivation of high-velocity SP is general and may be applied within a linear response treatment for other types of extended multicharged projectiles as well as for any particular form of the linear response function $\varepsilon(z,u)$ for the target material. For given target material this approach requires only the asymptotic form of the plasmon dispersion relation at high $u=\omega/kv_F$. In particular, for heavy energetic ions our method has been previously applied using the Brandt-Kitagawa variational statistical approximation for the structure factor of projectile ion (see Ref. [8] for detail).

We shall make some brief remarks on the RTA in the linear response function. In the literature on SP and related problems, the disorder (collision)-inclusive linear response function containing in the RTA, which is often referred to as the Mermin dielectric function, has so far been considered only in RPA. Going beyond RPA with electron-electron interaction and disorder treated at the same microscopic level is a difficult task. We may mention that recently the linear response function has been considered in RTA which conserves the particle number, momentum and energy (see Refs. [27,28] and references therein). The resulting dielectric function is somewhat involved and has not yet been much used.

[1]After completing our work we became aware of a paper by Kaneko [26] in which the high-velocity limit an extended ion SP has been investigated using the Brandt-Kitagawa model of the ion and within RPA but without disorder. The scope of our investigation is larger than in Ref. [26]. Where our work makes some contact with Ref. [26] we find that Kaneko's results are consistent with ours if we consider $\gamma=0$ in our results. Kaneko's work furnishes only the modified Bethe-Bohr logarithmic term while our results in Eqs. (63) and (65) contain also high-velocity corrections to the basic logarithmic SP.

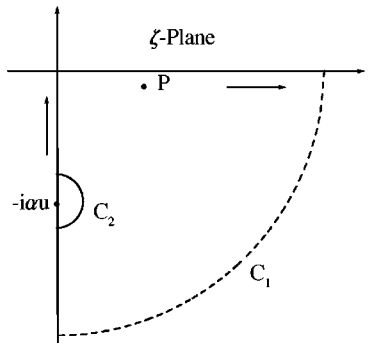

FIG. 7. Illustration of contour C_1 in the complex ζ plane. Isolated point P below the real ζ axis indicates the plasmon pole.

In our calculations of SP and related quantities we have modelled the disordered target medium as an electron gas whose linear response function is constructed in RTA in order to include scattering of electrons with disorder impurities. In our theory the phenomenological quantity γ is the inverse of the electron relaxation time. The numerical values of γ used in our calculations are within a physically expected range for the specific target medium. In principle γ can be calculated to varying degrees of approximations. In the simplest approximation, its inverse can be calculated through Fermi's golden rule for a model electron-impurity potential. This may allow us to see how SP and related quantities depend on the target properties through their influence on γ.

We expect our theoretical findings to be useful in experimental investigations of ion beam energy losses in solids. One of the improvements of our model will be to include some short-range correlation in the linear response function. A study of this and other aspects will be reported elsewhere.

ACKNOWLEDGMENTS

It is a pleasure to thank Professor C. Deutsch and Dr. G. Zwicknagel who directed us to some useful references.

APPENDIX A: EVALUATION OF FUNCTIONS $\Lambda_0(u)$ AND $\Lambda_1(\alpha,u)$

For a calculation of the functions $\Lambda_0(u)$ and $\Lambda_1(\alpha,u)$ at $u \gg 1$, it is convenient to introduce the following contour integral:

$$I=\int_{C_1}\left(1-\frac{1}{\varepsilon_1(\zeta,u,\Gamma)}\right)\frac{\zeta d\zeta}{\zeta^2+\alpha^2u^2}, \tag{A1}$$

where we introduce the new variable according to $\zeta=zu$ and $\varepsilon_1(\zeta,u,\Gamma)=\varepsilon(\zeta/u,u,\Gamma)$. The integration contour C_1 is shown in Fig. 7. This contour contains the real ζ axis $(0, +\infty)$, the lower quarter circle, the imaginary ζ axis $(-i\infty,0)$ and an infinitesimal semicircle C_2. In order to calculate the integral I, we have to know the poles of $1/\varepsilon_1(\zeta,u,\Gamma)$, i.e., the zeros $\zeta_r(u)=uz_r(u)$ of $\varepsilon_1(\zeta,u,\Gamma)$, for a fixed u. The solution of the plasmon dispersion equation for a disordered DEG has been investigated in detail in Ref. [19]. It has been

shown that $\zeta_r(u)$ lies in the lower quarter of the complex ζ plane as shown in Fig. 7 with an isolated point P below the real ζ axis.

For large values of $|z|$, the dielectric function must behave as $\varepsilon(z,u,\Gamma)\to 1+\chi^2/3z^4$ according to Ref. [19]. Therefore the integral I vanishes within the lower quadrants, and from Eqs. (47) and (A1) we find by evaluating the residues at the poles

$$\Lambda_1(\alpha,u)=2\pi\mathrm{Re}\left[\frac{\zeta_r(u)}{\partial\varepsilon_1(\zeta_r(u),u,\Gamma)/\partial\zeta}\frac{u^2}{\zeta_r^2(u)+u^2\alpha^2}\right]-\frac{\pi u^2}{2}\left[1-\frac{1}{S(\alpha,u)}\right], \tag{A2}$$

where $U=u-\Gamma/\alpha$,

$$S(\alpha,u,)=\varepsilon(-i\alpha,u,\Gamma)=1+\frac{(\alpha u-\Gamma)[S_R(\alpha,u,\Gamma)-1]}{\alpha u-\Gamma Q(\alpha,u,\Gamma)}, \tag{A3}$$

$$Q(\alpha,u,\Gamma)=\frac{S_R(\alpha,u,\Gamma)-1}{S_R^0(\alpha)-1}, \tag{A4}$$

$$S_R(\alpha,u,\Gamma)=1+\frac{\chi^2}{2\alpha^2}\left\{\frac{U^2-\alpha^2-1}{2\alpha}\left(\arctan\frac{\alpha}{U+1}-\arctan\frac{\alpha}{U-1}\right)+\frac{U}{2}\ln\frac{(U+1)^2+\alpha^2}{(U-1)^2+\alpha^2}-1\right\}, \tag{A5}$$

$$S_R^0(\alpha)=1-\frac{\chi^2}{2\alpha^2}\left\{\frac{1+\alpha^2}{\alpha}\arctan\alpha+1\right\}. \tag{A6}$$

It should be noted that Eqs. (A3)–(A6) follow directly from our analytical results, Eqs. (9)–(14), obtained for the dielectric function of a disordered DEG. Equation (A2) provides an explicit expression for the function $\Lambda_1(\alpha,u)$. It is now easy to evaluate the function $\Lambda_0(u)$ directly from Eq. (A2). We then obtain

$$\Lambda_0(u)=2\pi\mathrm{Re}\left[\frac{\zeta_r(u)}{\partial\varepsilon_1(\zeta_r(u),u,\Gamma)/\partial\zeta}\right]. \tag{A7}$$

For a calculation of asymptotic values of the functions in Eqs. (A2) and (A7) we must know the asymptotic expansion for large u of $\zeta_r(u)$ and also for $\varepsilon_1(\zeta_r(u),u,\Gamma)$. The expressions for these functions have been found in Ref. [19]. We recall that

$$\zeta_r(u)=\zeta_0+\frac{\tilde{\zeta}_2}{u^2}+\frac{\tilde{\zeta}_4}{u^4}+\cdots, \tag{A8}$$

where the coefficients ζ_0, $\tilde{\zeta}_2$, and $\tilde{\zeta}_4$ are independent on u and are found from Ref. [19]. Finally, using the analytical results obtained in Ref. [19] we arrive at Eq. (51).

APPENDIX B: EVALUATION OF L_0 FOR EXTENDED ION

In this appendix we give detail derivation of the parameter L_0 which contributes to the leading logarithmic term of high-velocity SP. First we write Eq. (49) in another but equivalent form,

$$L_0=\int_{z_{\min}}^{z_{\max}}\mathcal{Z}^2(z,\alpha)\frac{dz}{z}-q_1^2(2+\sigma_1)\ln z_{\max}+q_1^2(I_1-I_2), \tag{B1}$$

where we introduce the cutoff parameters $z_{\max}\to\infty$ and $z_{\min}\to 0$,

$$\sigma_1=\frac{1}{q_1^2}-1,\ln\sigma_2=\frac{q}{q_1^2}\left(1-\frac{11q}{12}\right), \tag{B2}$$

$$I_1=\frac{6}{\pi\chi^2q_1^2}\int_0^{z_{\max}}udu\int_0^{z_{\min}}\mathcal{Z}^2(\alpha,z)\mathrm{Im}\frac{-1}{\varepsilon(z,u,\Gamma)}zdz, \tag{B3}$$

$$I_2=\frac{6}{\pi\chi^2q_1^2}\int_{z_{\max}}^{\infty}udu\int_{z_{\min}}^{z_{\max}}\mathcal{Z}^2(\alpha,z)\mathrm{Im}\frac{-1}{\varepsilon(z,u,\Gamma)}zdz. \tag{B4}$$

For derivation of Eq. (B1) the Bethe sum rule in variables z and u has been used,

$$\int_0^{\infty}\mathrm{Im}\frac{-1}{\varepsilon(z,u,\Gamma)}udu=\frac{\pi\chi^2}{6z^2}. \tag{B5}$$

From Eq. (B1) at $z_{\max}\to\infty$ and $z_{\min}\to 0$ we find

$$\begin{aligned}\int_{z_{\min}}^{z_{\max}}\mathcal{Z}^2(z,\alpha)\frac{dz}{z}&=\ln\frac{z_{\max}}{z_{\min}}+Z^{-2}\hat{\mathcal{Z}}(\alpha)\int_{z_{\min}}^{z_{\max}}\frac{dz}{z(z^2+\alpha^2)}=\ln\frac{z_{\max}}{z_{\min}}\\&+Z^{-2}\hat{\mathcal{Z}}(\alpha)\left[\frac{1}{\alpha^2}\left(\ln\frac{z_{\max}}{z_{\min}}-\frac{1}{2}\ln\frac{z_{\max}^2+\alpha^2}{z_{\min}^2+\alpha^2}\right)\right]\\&=q_1^2\ln\frac{z_{\max}\sigma_2}{z_{\min}}+q_1^2\sigma_1\ln\frac{z_{\max}}{\alpha}.\end{aligned} \tag{B6}$$

Substituting this result into Eq. (B1) we obtain

$$L_0=q_1^2\ln\left(\frac{\sigma_2}{\alpha^{\sigma_1}}\frac{e^{-Q(\eta)}}{z_{\min}z_{\max}}\right), \tag{B7}$$

where $Q(\eta)=I_2(\eta)-I_1(\eta)$. Here as in Ref. [4] we assume that $z_{\max}=s$ and $z_{\min}=z_r(s)$, where $z_r(s)$ is the solution of dispersion equation for plasmons without damping and s is some free and large parameter. It is known (see, e.g., Refs. [4,19]) that at $s\to\infty$, $z_r(s)\to\chi/s\sqrt{3}\to 0$. Therefore $z_{\max}z_{\min}\to\chi/\sqrt{3}$at large s. Now we calculate the functions I_1 and I_2. After some transformation from Eqs. (B3) and (B4) at $s\to\infty$ we find

$$I_1(\eta)=\frac{4\eta}{\pi}\int_0^1\frac{dz}{z}\int_0^z\frac{u^2du}{u^4-2(1-2\eta^2)u^2+1}, \tag{B8}$$

$$I_2(\eta) = \frac{4\eta}{\pi}\int_1^\infty \frac{dz}{z}\int_z^\infty \frac{u^2 du}{u^4 - 2(1-2\eta^2)u^2 + 1}, \tag{B9}$$

where $\eta = \Gamma\sqrt{3}/2\chi$. The integrals over variable u can be calculated as follows:

$$\int_0^z \frac{u^2 du}{u^4 - 2(1-2\eta^2)u^2 + 1} = \frac{1}{4\eta\sqrt{1-\eta^2}}\mathrm{Im}\left[\tau \ln\frac{\tau - z}{\tau + z}\right], \tag{B10}$$

$$\int_z^\infty \frac{u^2 du}{u^4 - 2(1-2\eta^2)u^2 + 1} = -\frac{1}{4\eta\sqrt{1-\eta^2}}\mathrm{Im}\left[\tau \ln\frac{z - \tau}{z + \tau}\right], \tag{B11}$$

where $\tau = \sqrt{1-\eta^2} + i\eta$. The last expressions have been obtained under assumption that $\eta < 1$ (or $\gamma < 2\omega_p$) as it takes place for real disordered media.

Then after final integration over variable z we finally find

$$Q(\eta) = \frac{\eta}{\sqrt{1-\eta^2}}\arcsin\sqrt{1-\eta^2}. \tag{B12}$$

From Eq. (B12) it follows that the function $Q(\eta)$ increases with increasing of damping parameter Γ and at the value $\eta = 1 (\gamma = 2\omega_p)$, $Q(\eta) = 1$.

APPENDIX C: DERIVATION OF EQ. (73)

Substituting Eq. (72) into Eq. (67) we find the following expression for the coefficient K:

$$K(\lambda, R) = \frac{4Z^2\Sigma_0}{3\pi^2\chi^2\lambda^2}\sum_{n=n_1}^{n_2} \frac{n\kappa_n}{n^2 - \chi^2\delta^2/3}, \tag{C1}$$

where

$$\kappa_n = \left(1 + \frac{3}{10W_n}\right)\left[1 - \frac{q\alpha^4 x_n^2}{(\alpha^2 x_n + 1)^2}\right]^2, \tag{C2}$$

$x_n = 1/(W_n - 3/10)$, $W_n = \sqrt{9/100 + \lambda^2\zeta_n^2 - \chi^2/3}$, and $\delta = \rho/\lambda$. In Eq. (C1) $n_1 = 1 + E[\chi\rho/\nu(\lambda)\sqrt{3}]$, $n_2 = E[\nu(\lambda)\rho] \geqslant n_1$ with

$$\nu^2(\lambda) = \frac{1}{2}\left[\lambda^2 - \frac{3}{5} + \sqrt{\left(\lambda^2 - \frac{3}{5}\right)^2 - \frac{4\chi^2}{3}}\right]. \tag{C3}$$

The expression for $K(\lambda, R)$ given by Eq. (C1) is valid for $\lambda > \lambda_{\min}$ (when $\lambda < \lambda_{\min}$ this expression vanishes), where

$$\lambda_{\min}^2 = \frac{3}{5} + \frac{B^2(\rho) + 4\chi^2/3}{2B(\rho)}, \tag{C4}$$

and

$$B(\rho) = \frac{2\chi}{\sqrt{3}} + \frac{1}{\rho^2}\left(1 + \sqrt{1 + \frac{4\chi\rho^2}{\sqrt{3}}}\right). \tag{C5}$$

Note that from the condition $\lambda > \lambda_{\min}$ one can estimate, for a given and fixed ion velocity, the minimum distance $R_{\min}$ between ions discussed in Sec. III D.

An evaluation of the sum in Eq. (C1) is facilitated if we write it in an equivalent form,

$$K(\lambda, R) = \frac{4Z^2\Sigma_0}{3\pi^2\chi^2\lambda^2}[C + \ln n_2 + G_1(\alpha,\lambda) + G_2(\alpha,\lambda)], \tag{C6}$$

where

$$G_1(\alpha,\lambda) = \sum_{n=n_1}^{n_2}\frac{1}{n} - \ln n_2 - C, \tag{C7}$$

$$G_2(\alpha,\lambda) = \sum_{n=n_1}^{n_2}\frac{1}{n}\left(\frac{n^2\kappa_n}{n^2 - \chi^2\delta^2/3} - 1\right). \tag{C8}$$

In the limit $\lambda \gg 1$ we can have, to the leading order, $x_n \cong 1/\lambda\zeta_n$, $n_1 = 1$, $n_2 \cong \lambda\rho \gg 1$. Therefore, using the asymptotic result for the sum $G_1(\alpha,\lambda)$ [29], we obtain

$$G_1(\alpha,\lambda) = \frac{1}{2n_2} - \frac{1}{12n_2^2} + O(n_2^{-3}) = \frac{1}{2\lambda\rho} - \frac{1}{12\lambda^2\rho^2} + O\left(\frac{1}{\lambda^3\rho^3}\right). \tag{C9}$$

In a high-velocity limit $G_2(\alpha,\lambda)$ is approximated as

$$G_2(\alpha,\lambda) \cong \frac{3\rho}{10\lambda}\sum_{n=1}^{n_2}\frac{1}{n^2} - \frac{\rho^2}{\lambda^2}\left(2q\alpha^4 - \frac{\chi^2}{3}\right)\sum_{n=1}^{n_2}\frac{1}{n^3}. \tag{C10}$$

Both the sums in Eq. (C10) can be expressed in terms of the dilogarithm function [29]. In a high-velocity limit when $n_2 \cong \lambda\rho \gg 1$, using the asymptotic expressions for this function we find that the first and second sums are equal to $\pi^2/6 - 1/\lambda\rho$ and $\zeta(3)$, respectively. Hence

$$G_2(\alpha,\lambda) \cong \frac{\pi^2\rho}{20\lambda} - \frac{1}{\lambda^2}\left[\frac{3}{10} + \rho^2\zeta(3)\left(2q\alpha^4 - \frac{\chi^2}{3}\right)\right]. \tag{C11}$$

Taking into account that $\ln n_2 \cong \ln(\lambda\rho) - 3/10\lambda^2$, we finally arrive at Eq. (73).

[1] C. Deutsch, Ann. Phys. (Paris) **1**, 111 (1986); Laser Part. Beams **2**, 449 (1984); Laser Part. Beams **8**, 541 (1990); Phys. Rev. E **51**, 619 (1995).
[2] N. R. Arista and W. Brandt, Phys. Rev. A **23**, 1898 (1981); T. A. Mehlhorn, J. Appl. Phys. **52**, 6522 (1981); N. R. Arista and A. R. Piriz, Phys. Rev. A **35**, 3450 (1987).
[3] Proceedings of the 13th International Symposium on Heavy Ion Interial Fusion San Diego, CA, 2000, edited by E. Lee, C. Celata, J. Barnard, D. Callahan-Miller, S. Lund, A. Molvik, P. Peterson, and I. Haber [Nucl. Instrum. Methods Phys. Res. B 464 (2001)].
[4] J. Lindhard, K. Dan. K. Dan. Vidensk. Selsk. Mat. Fys. Medd. **28**, 1 (1954); J. Lindhard and A. Winther, *ibid.* **34**, 1 (1964).
[5] J. F. Ziegler, J. Appl. Phys. **85**, 1249 (1999).
[6] G. Zwicknagel, C. Toepffer, and P.-G. Reinhard, Phys. Rep. **309**, 117 (1999).
[7] H. B. Nersisyan and A. K. Das, Phys. Rev. E **62**, 5636 (2000).
[8] H. B. Nersisyan and A. K. Das, Nucl. Instrum. Methods Phys. Res. B **205**, 281 (2003).
[9] N. D. Mermin, Phys. Rev. B **1**, 2362 (1970).
[10] A. K. Das, J. Phys. F: Met. Phys. **5**, 2035 (1975).
[11] I. Abril, R. Garcia-Molina, and N. R. Arista, Nucl. Instrum. Methods Phys. Res. B **90**, 72 (1994); F. J. Perez-Perez, I. Abril, N. R. Arista, and R. Garcia-Molina, *ibid.* **115**, 18 (1996); F. J. Perez-Perez, I. Abril, R. Garcia-Molina, and N. R. Arista, Phys. Rev. A **54**, 4145 (1996).
[12] J. C. Ashley, Nucl. Instrum. Methods **170**, 197 (1980).
[13] J. C. Ashley and P. M. Echenique, Phys. Rev. B **35**, 8701 (1987).
[14] J. C. Ashley and P. M. Echenique, Phys. Rev. B **31**, 4655 (1985).
[15] G. Zwicknagel, C. Toepffer, and P.-G. Reinhard, Laser Part. Beams **13**, 311 (1995).
[16] G. Zwicknagel, C. Deutsch, Laser Part. Beams **14**, 749 (1996).
[17] A. Selchow and K. Morawetz, Phys. Rev. E **59**, 1015 (1999); A. Selchow, G. Röpke, and K. Morawetz, Nucl. Instrum. Methods Phys. Res. A **441**, 40 (2000).
[18] H. B. Nersisyan and A. K. Das. Phys. Lett. A **296**, 131 (2002).
[19] H. B. Nersisyan, A. K. Das, and H. H. Matevosyan, Phys. Rev. E **66**, 046415 (2002).
[20] G. Basbas and R. H. Ritchie, Phys. Rev. A **25**, 1943 (1982).
[21] C. Deutsch and P. Fromy, Phys. Lett. A **198**, 347 (1995); C. Deutsch, P. Fromy, and G. Zwicknagel, Laser Part. Beams **14**, 699 (1996); G. Zwicknagel and C. Deutsch, Phys. Rev. E **56**, 970 (1997); Nucl. Instrum. Methods Phys. Res. A **415**, 599 (1998); G. Zwicknagel, Ph.D. thesis, University of Erlangen, 2000.
[22] N. R. Arista and E. M. Bringa, Phys. Rev. A **55**, 2873 (1997).
[23] N. P. Wang and I. Nagy, Phys. Rev. A **55**, 2083 (1997).
[24] P. M. Echenique, F. Flores, and R. H. Ritchie, Solid State Phys. **43**, 229 (1990).
[25] S. P. Møller, A. Csete, T. Ichioka, H. Knudsen, U. I. Uggerhøj and H. H. Andersen, Phys. Rev. Lett. **88**, 193201 (2002).
[26] T. Kaneko, Nucl. Instrum. Methods Phys. Res. B **48**, 83 (1990).
[27] K. Morawetz and U. Fuhrmann, Phys. Rev. E **61**, 2272 (2000); **62**, 4382 (2000).
[28] G. S. Atwal and N. W. Ashcroft, Phys. Rev. B **65**, 115109 (2002).
[29] I. S. Gradshteyn and I. M. Ryzhik, *Table of Integrals, Series and Products* (Academic, New York, 1980).